# WAVE-INDUCED
# WATER PARTICLE MOTION MEASUREMENTS

Richard Francis Krapohl

# NAVAL POSTGRADUATE SCHOOL
## Monterey, California


# THESIS

WAVE-INDUCED

WATER PARTICLE MOTION MEASUREMENTS

by

Richard Francis Krapohl

Thesis Advisor: E.B. Thornton

December 1972

# Wave-Induced

# Water Particle Motion Measurements

by

Richard Francis Krapohl
Lieutenant, United States Navy
B.S., United States Naval Academy, 1967

Submitted in partial fulfillment of the
requirements for the degree of

MASTER OF SCIENCE IN OCEANOGRAPHY

from the

NAVAL POSTGRADUATE SCHOOL
December 1972

ABSTRACT

Simultaneous measurements of wave height and two orthogonal water particle velocities were made at six elevations in nineteen meters of water using a penetrating wave staff and an electromagnetic flowmeter. Moderate swell and low wind conditions prevailed during the experiment. The measured wave-induced velocities were two to four percent greater than those predicted using linear wave theory. Coherence of the wave height and wave-induced velocities in the significant energy-density range was computed to be over 0.85, indicating that the motion was almost totally wave induced. At higher frequencies it was apparent that the motion was primarily turbulence. Phase spectra computed for the measured wave heights and orbital velocities compared very well with linear theory. Measured frequency distributions were compared to both Gaussian and Gram-Charlier distributions using the chi-squared goodness-of-fit test. Qualitatively, the Gram-Charlier distribution gave the better fit to the data.

TABLE OF CONTENTS

## LIST OF TABLES

## LIST OF FIGURES

## LIST OF SYMBOLS

| | |
|---|---|
| $a$ | wave amplitude |
| $B$ | magnetic field intensity |
| $C$ | degrees centigrade |
| $C_{xy}(f)$ | co-spectrum |
| $E$ | induced electric potential |
| $f$ | frequency |
| $g$ | acceleration of gravity |
| $h$ | total water depth |
| $i$ | square root of -1 |
| $\vec{k}$ | horizontal vector wave number |
| $L$ | wave length |
| $m$ | meter |
| $P(\tau)$ | Parzen window function |
| $Q_{xy}(f)$ | quadrature spectrum |
| $s$ | seconds |
| $t$ | time |
| $u$ | horizontal component of orbital velocity |
| $v$ | horizontal component of orbital velocity orthogonal to u |
| $w$ | vertical component of orbital velocity |
| $W$ | amplitude of vertical orbital velocity |
| $x$ | horizontal coordinate |
| $z$ | vertical coordinate |
| $\gamma^2$ | coherence function |
| $\Delta$ | incremental difference |
| $\varepsilon$ | phase angle |

| | |
|---|---|
| $\sigma$ | angular wave frequency |
| $\tau$ | lag time |
| $\phi_{xx}(\tau)$ | auto-covariance function |
| $\phi_{xy}(\tau)$ | cross-covariance function |
| $\Phi_{xx}(f)$ | energy-density spectrum |
| $\Phi_{xy}(f)$ | cross-spectrum |

ACKNOWLEDGEMENT

The author wishes to take this opportunity to express his appreciation to the many who made this work possible. A complete list of people to which he is indebted is impossible but it is hoped that by naming a few individuals even those unnamed will know their efforts were appreciated.

Professor E.B. Thornton, his thesis advisor, was the real guiding light throughout this research and without his consummate effort this work could not have been completed.

The personnel of the Naval Postgraduate School's machine facility provided timely and invaluable assistance in preparation for the field work. The technicians at the NUC tower proved themselves to be indispensable during the data taking, while the data processing in such a short period of time would not have been possible without the extraordinary assistance of the employees of the W.R. Church Computer Center at the Naval Postgraduate School.

Finally, and most importantly to my wife Kay, for her patience and devotion through repeated manuscript typings, and nights spent away from home, a most grateful, thank you.

# I. INTRODUCTION

## A. BACKGROUND

Measuring instantaneous water particle velocities in the presence of wave-induced motion has been difficult due, primarily, to a lack of instrumentation. This is particularly true for measurements made in the field. Until recently, there has been no adequate instrument available to measure rapidly fluctuating flows found beneath wind waves and swell. As well as the usual requirements of reliability and accuracy, such an instrument must also be rugged, have a low response time, and have good directional measuring characteristics.

Earlier attempts at correlating water height and particle motion have generally been accomplished in shallow water next to the shore, off piers, or in estuaries. Historically, Inman and Nasu (1956) made one of the earliest attempts at field measurements of wave-induced water particle motion, using a force meter in shallow water and compared their results to solitary wave theory. Miller and Zeigler (1964) used both an acoustic meter (based on the doppler shift principle) and an electromagnetic flowmeter to measure water particle motion in the surf zone. They compared their measurements to higher order wave theory and obtained qualitative agreement.

Nagata (1963, 1964a, 1964b) used an electromagnetic flowmeter in a series of experiments to measure water

particle velocities in the surf zone and to determine wave directional spectra. Bowden and White (1966) and Simpson (1968) performed field measurements using an electromagnetic flowmeter developed at the National Institute of Oceanography. Like Nagata, Bowden and White (1966) used water particle velocities to determine the directional spectrum of waves.

Simpson's experiment was performed at an open coastal site in water approximately 6 meters deep. The waves, primarily wind generated sea waves, were developed over a limiting fetch of 210 km. Simpson employed spectral methods in the analysis of the waves and of the wave-induced water particle velocities. His results were consistent with linear wave theory.

Seitz (1971) carried out a similar experiment in that he measured sea surface displacement and water velocity components in an estuary at a depth of one meter. He compared the measured velocity spectra to a derived velocity spectra obtained from direct measurement of the surface wave field using linear theory. Seitz had to contend with a shift in the observed frequencies, the magnitude of which was a function of the tide induced velocity. Since at the frequency of peak amplitude the error introduced was approximately 6.7%, he did not correct the data. The total water particle motion at depth can be described as the sum of the turbulent velocities and the surface wave induced motion. Seitz attempted to separate the two based on the slope of the spectrum in the inertial sub-range.

The lack of instrumentation has not been the only hindrance to wave height and velocity studies. Most research has been conducted at shallow water inshore sites because of the general unavailability of a deep water, exposed instrument platform. Shonting (1966) used the Buzzard's Bay Entrance Light Station on the South Coast of Massachusetts to obtain a twenty meter water depth at an open ocean site. He used ducted current meters to measure the orthogonal components of the water velocity under waves. His experiment was designed primarily to evaluate these meters. An inherent difficulty with any type of ducted meter is their poor directional measuring characteristics when the angle between meter axis and the flow is large.

Bordy (1971) made measurements in 20 meters of water from the Naval Undersea Research and Development Center (NUC) Oceanographic Research Tower located approximately one mile off Mission Beach, San Diego. He compared wave height and water particle velocity using spectral analysis, and found a general agreement with linear wave theory except for measurements of phase spectra at the deepest measurements of ten meters. The phase shift encountered was unexplained in the phase angle error analysis. During the experiment, the NUC tower's permanently installed wave staff system was used for water level sensing. The flowmeter was removed horizontally from the wave staff by approximately five feet. It is felt that due to this displacement, an error was introduced.

During 8 June 1972 records of orthogonal water particle velocity and instantaneous water elevation were again measured at the NUC tower. The data were taken in conjunction with an experiment involving the investigation of wave induced fluctuations in acoustic phase shifts, temperature, and salinity.

The results of the wave and water particle motion measurements are described here. An electromagnetic flowmeter was used to gather the wave particle velocity data at several depths. These measured values of wave-induced motion were compared with values predicted using linear theory and the wave height record.

## B. RESEARCH OBJECTIVE

The purpose of this investigation was four fold:

1. To measure simultaneously wave height and two orthogonal wave-induced water particle velocities.

2. To perform a spectral analysis on the data to obtain its statistical properties.

3. To spectrally compare the data to first order wave theory.

4. To determine the statistical geometry of both the sea surface and the measured velocities.

## II. EXPERIMENTAL SITE AND INSTRUMENTATION

### A. EXPERIMENTAL SITE

The experiment was conducted at the Naval Undersea Research and Development Center Oceanographic Research Tower at San Diego, California, 8 and 9 June 1972. The NUC tower is located approximately one mile off Mission Beach, San Diego in a mean water depth of 19 meters. It is constructed of steel and concrete and is permanently imbedded in the sea floor, Figure (1). The forty foot square tower has three levels. The first is used primarily for gaining access, while the second houses machinery and provides work space for placing instruments in the water. The third, which is enclosed, is used for the housing of electrical equipment and also provides sleeping space for six men. The legs of the tower slope five degrees. A pair of tracks is mounted on the north, south, and west sides for lowering scientific instrument packages into the sea to any depth above the ocean floor. The western side of the tower was used for the experiment because of its exposure to the predominant swell.

### B. INSTRUMENTATION

Water particle velocities were measured with an Engineering Physics Company water current meter Model EMCM-3B. The sea surface elevation was measured with a Baylor Company wave staff system Model 13528R. The penetrating wave measuring system gives a direct measure of the sea surface elevation.

Figure 1. Naval Undersea Research and Development Center Oceanographic Research Tower, San Diego, California

The model 13528R Baylor Company Wave Staff System is an instantaneous water level measuring device consisting of two tensioned 1/2", 6x19 IWRC 304 SS wire ropes. Together with these lengths of stainless steel wire rope, the transducer produces an electrically linear direct current output that is proportional to the amount of wave staff above a short circuit produced by the water surface. System accuracy is stated as within one percent of actual height and the time constant is less than 0.06 seconds.

As received from the manufacturers, the working length of the staff was 50 feet; however, in order to take water particle velocity measurements near the surface directly under the staff, it was shortened to 20 feet. After shortening, the staff was recalibrated. The resulting calibration curve is shown in Figure (2). The rails on which the instrument cart rides slopes with the legs of the tower. This necessitated the rigging of an aluminum "I" beam with a trolley to support the Baylor wave staff system directly over the electromagnetic flowmeter. The wave staff was tensioned by allowing the weight of the instrument cart and frame to be exerted on the lower end of the wave staff cables. The estimated tension was approximately 800 pounds. The instrument and installation are shown in Figure (3).

The EMCM-3B electromagnetic current measuring device measures two orthogonal components of water particle velocity through a range of zero to five M/SEC. Other characteristics of the flow meter are:

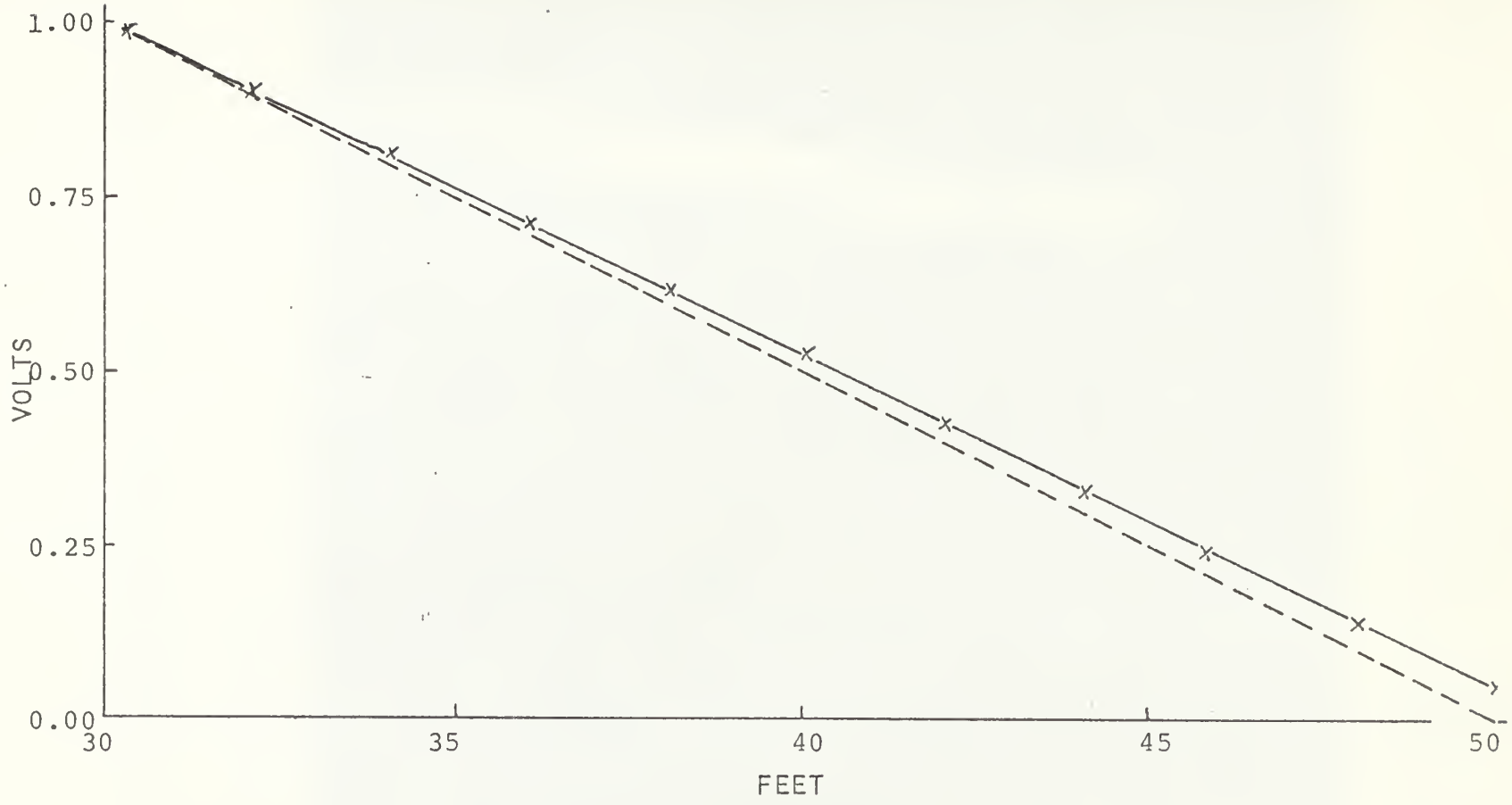


Figure 2. Calibration Curve for the Baylor Company Model 13528R Wave Staff System

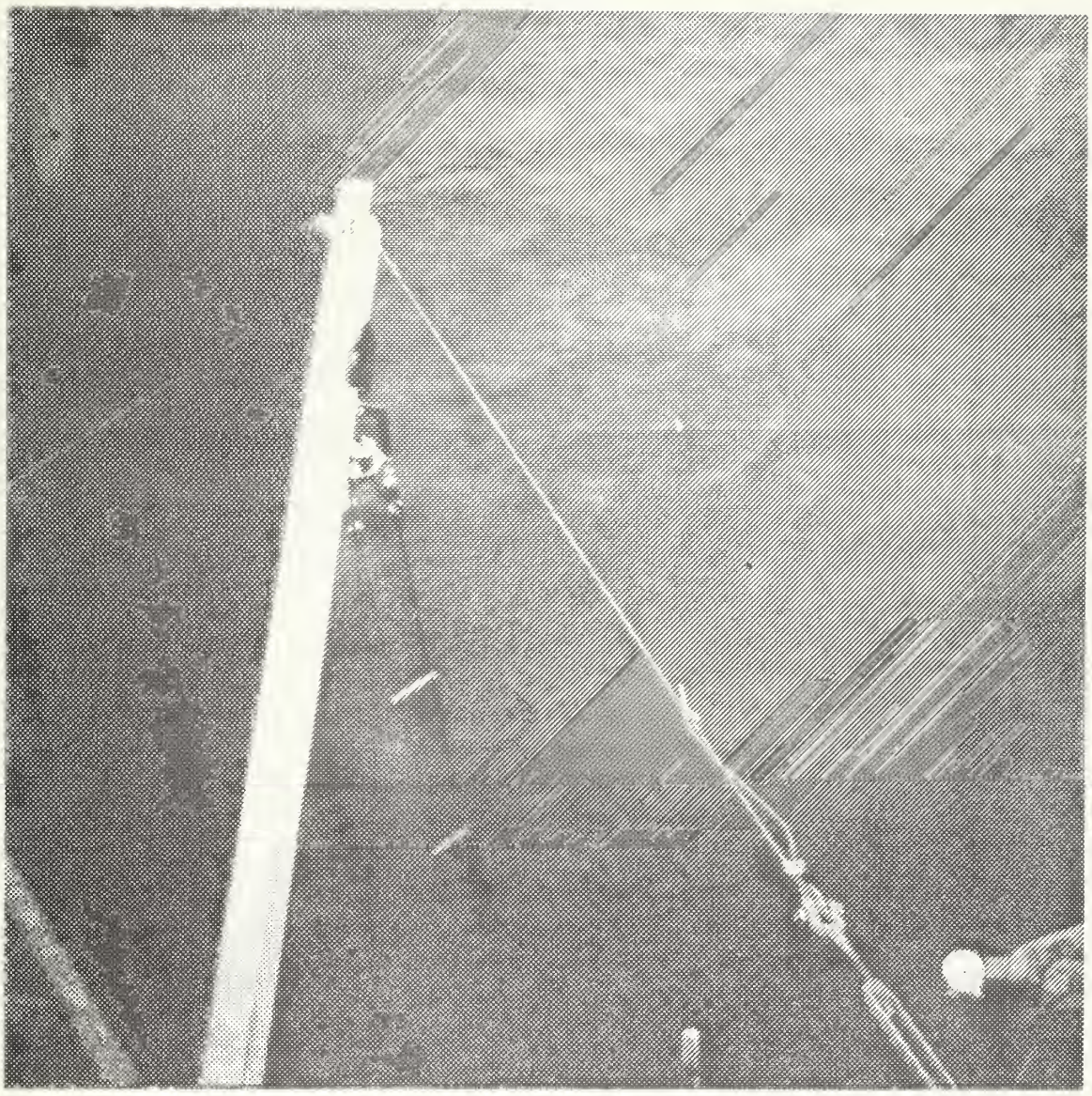

Figure 3. Model 13528R Baylor Company Wave Staff System

| | |
|---|---|
| Output Voltage: | ±5 volts full scale |
| Electrical Time Constant: | 0.2 seconds or longer, adjustable by user |
| Error Band: | the largest of<br>1) ±1 percent of full scale<br>2) ±5 MM/SEC<br>3) $5/(T^{\frac{1}{2}})$ MM/SEC<br>where T is the time constant |
| Transducer Size: | 2 3/4" O.D. x 36" L |

The operation of the unit is based on Faraday's principle of magnetic induction. A current is induced when a conducting fluid flows around the probe through an alternating magnetic field generated by a toroidal magnet inside the instrument. The equation describing the production of current is:

$$\vec{E} = \vec{u} \times \vec{B},$$

where $\vec{E}$ is the induced voltage, $\vec{u}$ the velocity of the conducting medium, and $\vec{B}$ the magnetic field. The induced electromotive force is linearly proportional to the amount of fluid flowing through the magnetic field. The magnetic field, $\vec{B}$, is most intense in the near vicinity of the probe and decreases according to the inverse square of the distance from the instrument. Accordingly, the flow velocity near the probe is weighted most heavily in its contribution to the measured velocity. Qualitatively, only that water which is within a distance of two to three probe radii contributes significantly to the flow induced voltage.

The flow meter was originally calibrated under steady flow conditions by the manufacturer. Different response characteristics are to be expected under unsteady flow conditions; consequently, the probe was recalibrated by oscillating it in a water tank. The equipment schematic is shown in Figure (4). The carriage on which the flow meter probe was mounted travels back and forth on rails. It is driven by a variable speed electrical motor. The peak carriage velocity was calculated from the tangential velocity of the motor arm. The ratio of carriage velocity, $V_t$, to the velocity measured by the instrument, $V_m$, was found for different angular velocities. This was done for each pair of electrodes by orienting them parallel to the flow in turn.

The instrument's response was very linear with respect to frequency up to at least 0.5 Hz. Beyond this frequency the cart upon which the probe was mounted became unstable. Thus 0.5 Hz was the maximum frequency investigated during calibration. This limitation was not deemed a debilitating factor since 0.5 Hz was above the upper frequency limit of significant wave energy. The results of the calibration are shown in Figure (5) and the instrument and installation in Figure (6).

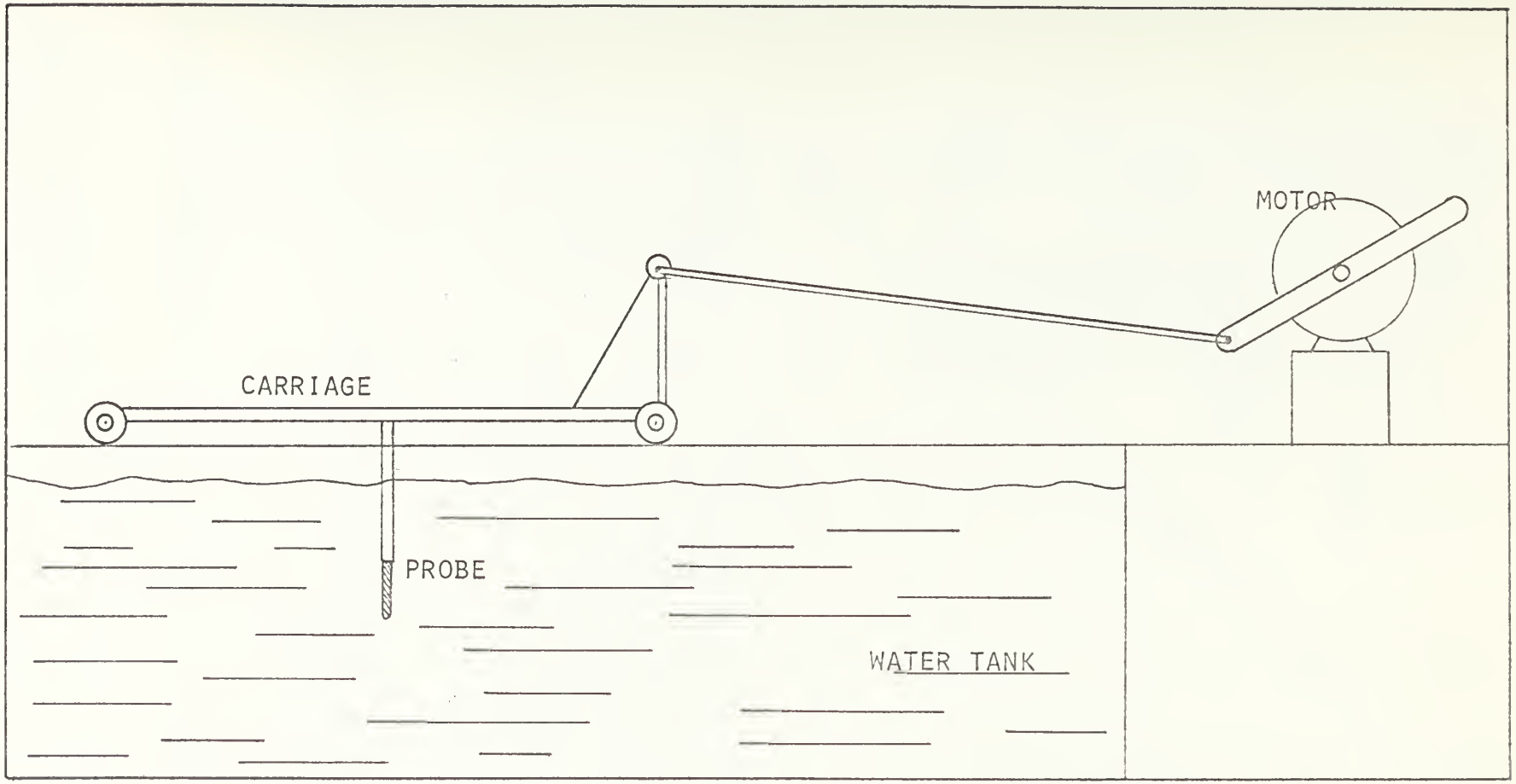


Figure 4. Schematic of Calibration Equipment for Flowmeter

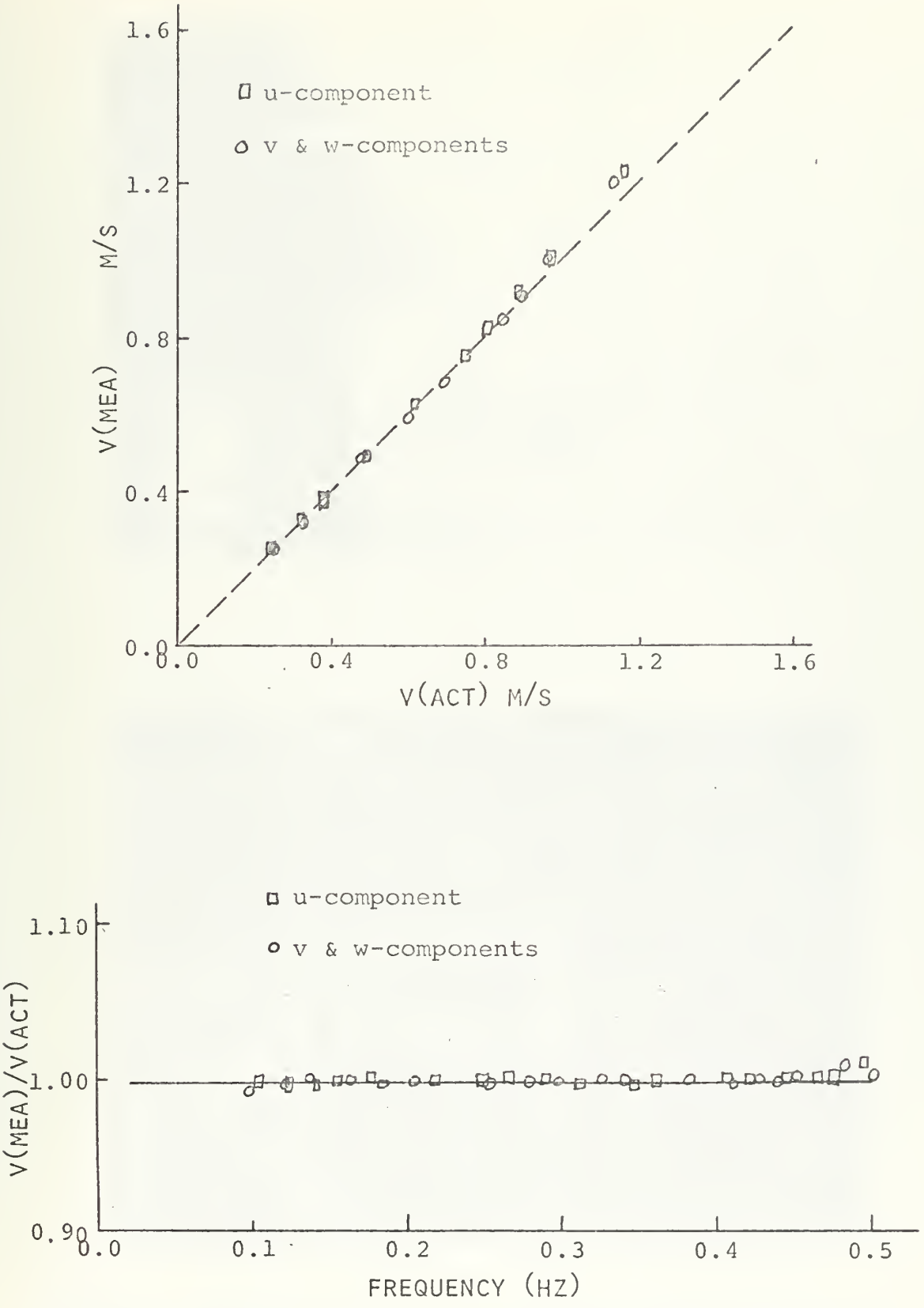


Figure 5. Calibration Curve for the Engineering Physics Company Model EMCM-3B Flowmeter

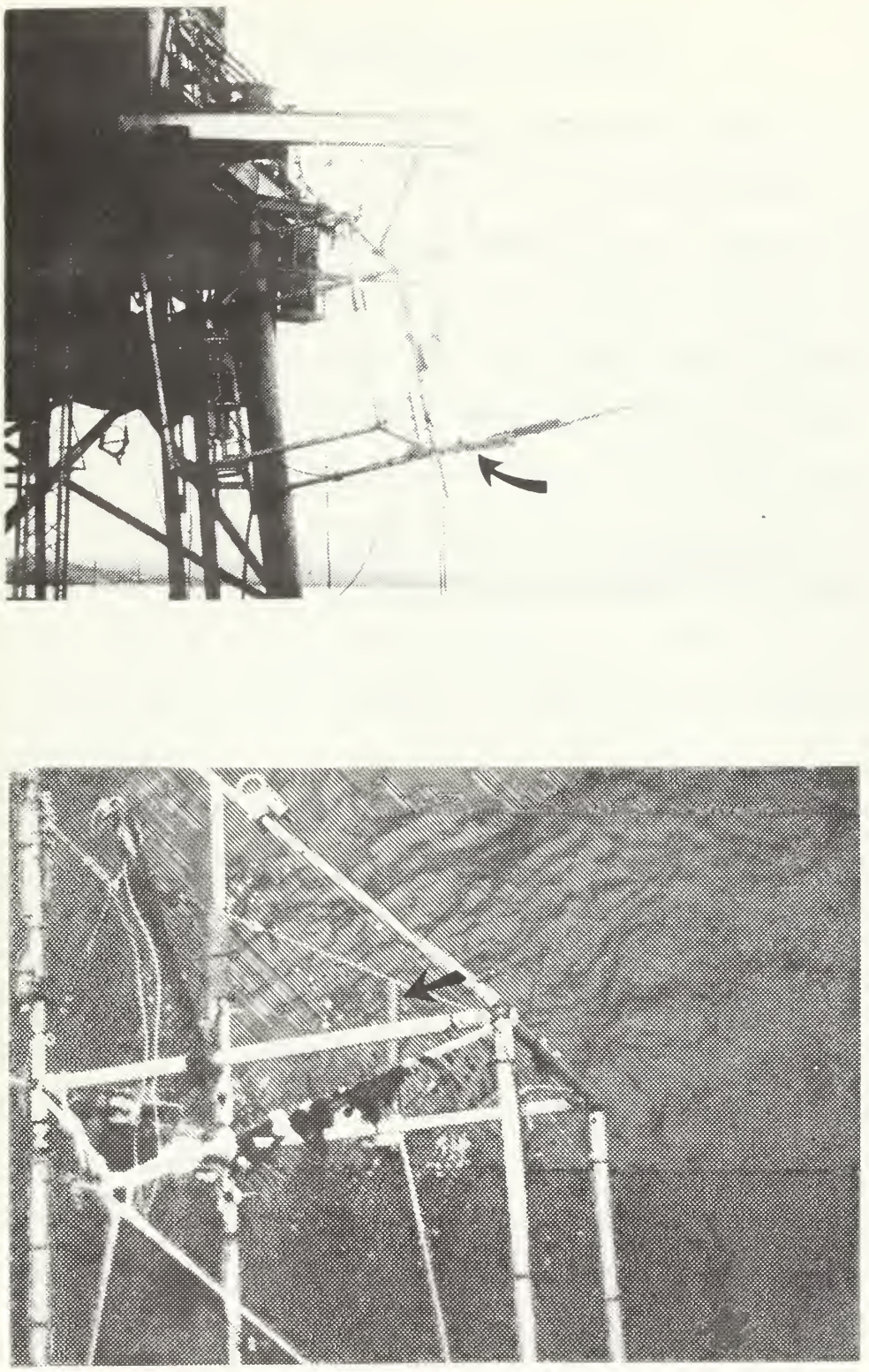

Figure 6. Engineering Physics Company Model EMCM-3B Electromagnetic Flowmeter Installed in Position (arrows) on the instrument cart

## III. EXPERIMENTAL PROCEDURE

Sea surface elevation and two orthogonal components of water particle velocity were measured simultaneously. The cart on which the flowmeter was attached was raised and lowered so that measurements could be made at various depths.

Data from the flowmeter and wave gauge were recorded on a Sangamo Model 3500 fourteen channel FM tape recorder during the ten data collection periods. The data chosen for analysis was obtained during the first six recording periods on 8 June 1972. Each processed run was about 20 minutes duration. After initial processing, the other four data collection periods were deemed too short to be statistically representative.

Summarized in Table I below are the velocity components, water depth, depth of the instrument, and record length for each of the processed runs. Instrument depth refers to the depth of the flowmeter below mean sea level. The u-component of velocity was oriented north-south approximately parallel to the shore, while the v-component was measured east-west. Correct flowmeter orientation was obtained using a plumb-bob and level. The wave gauge was always maintained directly over the flowmeter. As the cart was lowered the top of the wave staff was pushed further away from the tower to compensate for the five degree tilt of the tracks to which the cart was fastened.

The wave staff's perpendicularity to the horizontal was also ascertained by the use of a level. The wave staff installation is pictured in Figures (7) and (8).

TABLE I

| RUN | DEPTH (meters) | DEPTH OF INSTRUMENT (meters) | COMPONENT OF VELOCITY | LENGTH OF RECORDS (minutes) |
|---|---|---|---|---|
| 1 | 19.15 | 7.04 | u & v | 24.96 |
| 2 | 19.22 | 14.62 | u & w | 22.61 |
| 3 | 19.25 | 12.64 | u & w | 21.33 |
| 4 | 19.28 | 10.69 | u & w | 24.85 |
| 5 | 19.32 | 8.66 | u & w | 18.88 |
| 6 | 19.36 | 5.70 | u & w | 19.52 |

The sea surface was in general disturbed by swell coming from the west-southwest. The sky was overcast with a low stratus layer and little wind, less than 10 knots generally. Sea surface temperature was obtained using a bucket thermometer. Table II summarizes the environmental data.

TABLE II

| RUN | TIME OF START OF RUN (PDT) | AIR TEMP (°C) | SEA SURF TEMP (°C) | WIND DIR (°T) | WIND VEL (knots) | CLOUD COVER (%) | SWELL DIR |
|---|---|---|---|---|---|---|---|
| 1 | 1405 | 19.7 | 19.20 | 240 | 8 | 100 | WSW |
| 2 | 1600 | 19.6 | 18.95 | 250 | 10 | 100 | WSW |
| 3 | 1654 | 19.2 | 18.20 | 240 | 9 | 100 | WSW |
| 4 | 1800 | 18.7 | 19.10 | 225 | 6 | 100 | WSW |
| 5 | 1830 | 18.2 | 18.99 | 225 | 7 | 100 | WSW |
| 6 | 1922 | 17.9 | 18.77 | 235 | 4 | 100 | WSW |

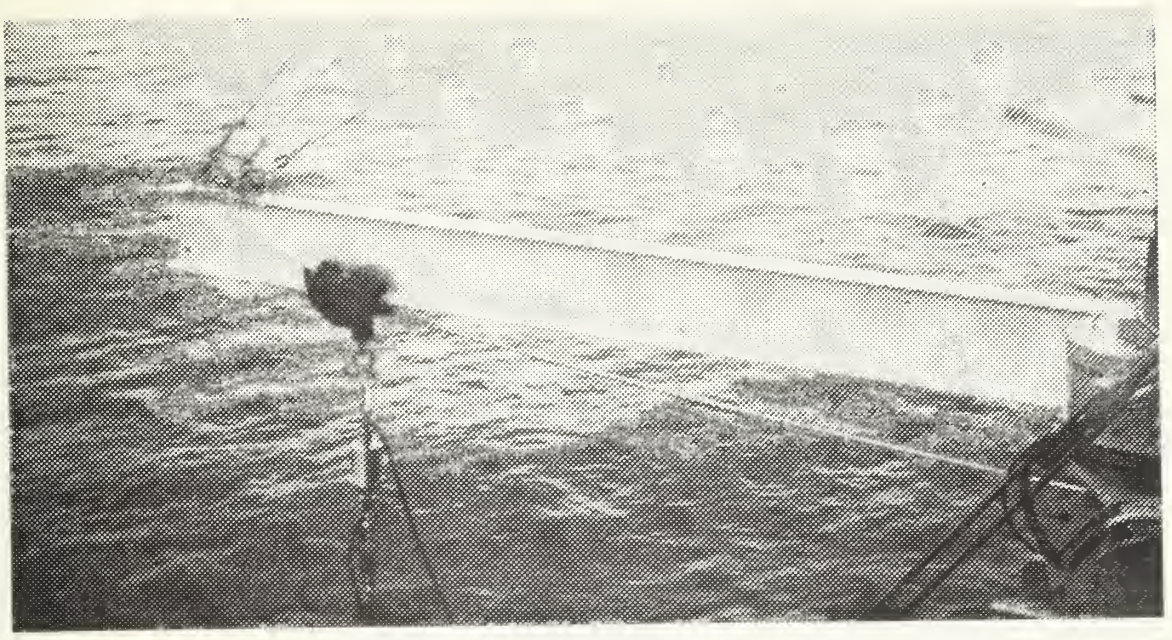

Figure 7. Model 13528R Baylor Wave Staff Installation Showing "I" Beam and Trolley for the Top of the System.

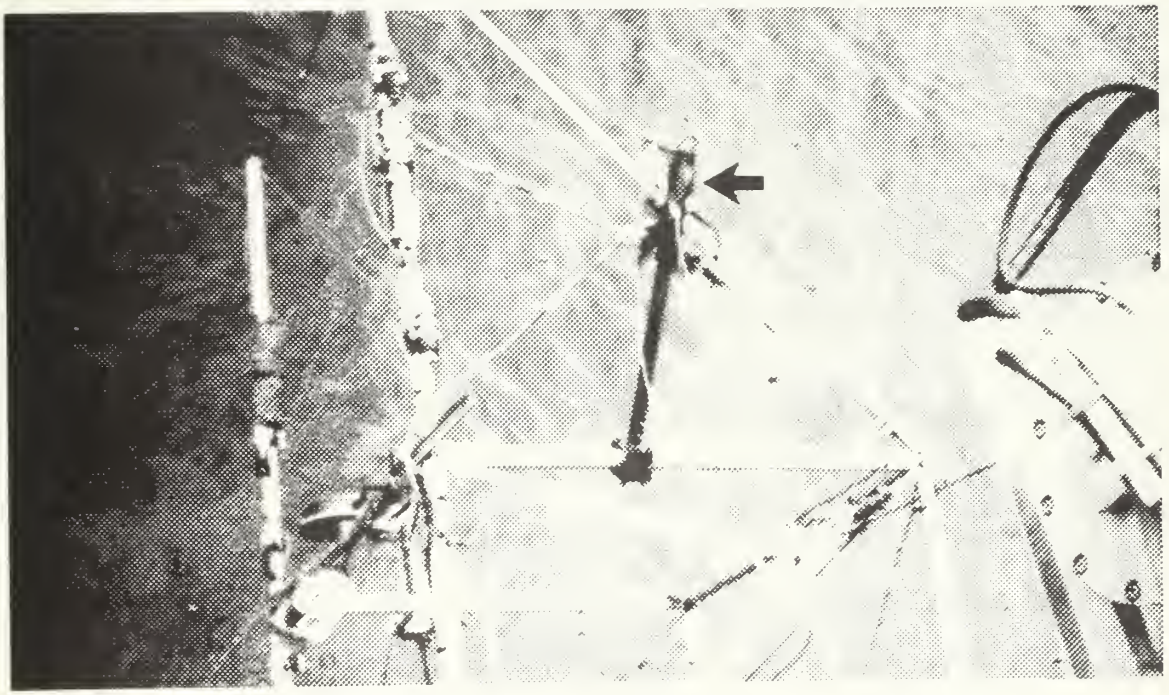

Figure 8. Pulley Attachment Point for the Bottom of the Baylor Wave Gauge (arrow).

Table III summarizes the temperature profile data taken at the beginning of each data collection period. This data, which shows a remarkable variation in layer depth and intensity of temperature gradient, was obtained using a mechanical BT. The NUC tower was originally constructed to study internal waves which are prevalent in the area. The variability in temperature profiles is attributed to internal waves. A typical temperature profile is shown in Figure (9).

TABLE III

| RUN | BT SURF TEMP(°C) | TOP OF 1st LAYER (°C/m) | BOTTOM OF 1st LAYER ("C/m) | TOP OF 2nd LAYER (°C/m) | BOTTOM TEMP (°C) |
|---|---|---|---|---|---|
| 1 | 22.8 | 22.2/7.31 | 16.6/12.19 | xxxxxxxxxx | 15.55 |
| 2 | 22.5 | 22.2/3.04 | 19.9/12.80 | 17.2/15.85 | 16.66 |
| 3 | 23.3 | 23.3/6.08 | 21.6/9.14 | 20.5/16.46 | 18.33 |
| 4 | 21.1 | 21.1/4.87 | 19.4/6.71 | 18.3/17.68 | 16.66 |
| 5 | 22.2 | 21.6/5.49 | 19.9/10.67 | 17.7/17.06 | 18.33 |
| 6 | 19.9 | 19.9/5.79 | 16.1/15.24 | xxxxxxxxxx | 16.11 |

The analog FM recordings were digitized using a hybrid system consisting of a Scientific Data Systems (SDS) Model 5000 analog computer and a Xerox Data Systems Model 9300 digital computer. For comparison purposes the data were transcribed onto a rectilinear eight channel Clevite strip chart recorder after a tenfold amplification through the (SDS) 5000 analog computer. An example of the transcribed data, after digitization, is shown in Figure (10). After

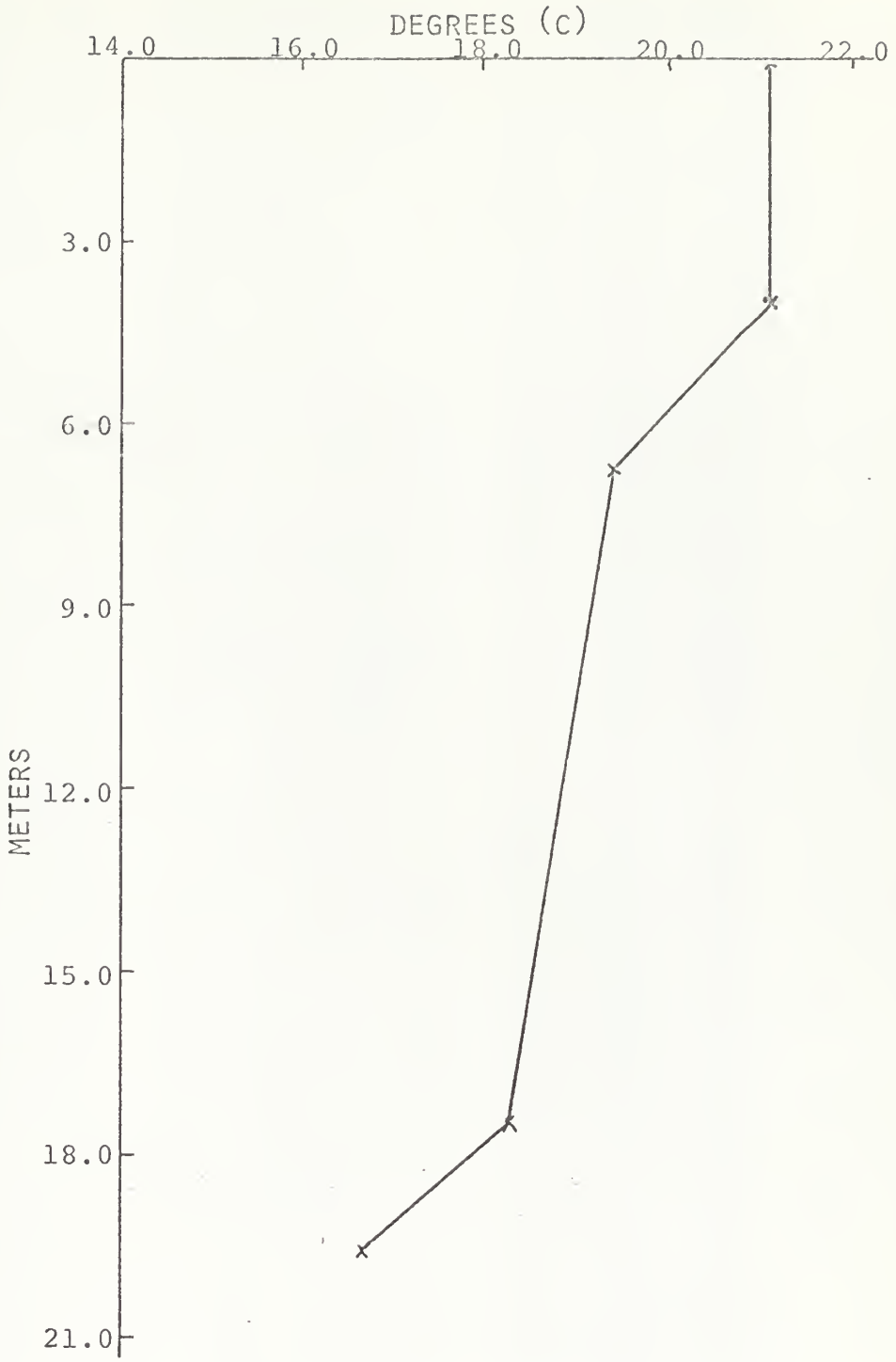


Figure 9. Typical Temperature-Depth Profile.
Run Number 4. 8 June 1972.


Figure 10. Transcribed Analog Data after Digitizing.

digitizing onto the seven track tape used by the 9300 system, the data were transcribed onto a nine track tape using the Naval Postgraduate School's IBM Model 360 digital computer. This computer was also used for the statistical analysis.

# IV. THEORY

## A. LINEAR WAVE THEORY

The elevation of the surface $\eta(t)$ can be described as the superposition of an infinite number of sinusoids of the form:

$$\eta(t) = \sum_{n=1}^{\infty} a_n \cos(\vec{k}_n \cdot \vec{x} - \sigma_n t + \varepsilon_n) = \sum_{n=1}^{\infty} \eta_n \tag{4.1}$$

where $\vec{x}$ is the horizontal Cartesian coordinate, t is the time, $\vec{k}$ is a horizontal vector wave number, $\sigma_n$ the frequency related in linear theory to $\vec{k}$ by:

$$\sigma_n^2 = gk_n \tanh k_n h \tag{4.2}$$

where g is the acceleration of gravity, $a_n$ is the amplitude and $\varepsilon_n$ the phase angle. $\eta(t)$ represents the sum total of all component wavelets. Summing in the manner of Equation (4.1) implies a linear system and restricts the analysis to the use of linear or Airy wave theory to describe the wave induced motion.

Linear wave theory can be used to predict the wave induced water particle velocities. The equations for the horizontal and vertical velocities respectively are:

$$u(t) = \sum_{n=1}^{\infty} \frac{a_n g k_n \cosh k_n(h+z)}{\sigma_n \sinh k_n h} \cos(\vec{k}_n \cdot \vec{x} - \sigma_n t + \varepsilon_n)$$

$$\text{or} \quad = \sum_{n=1}^{\infty} \frac{g k_n \cosh k_n(h+z)}{\sigma_n \sinh k_n h} \eta_n \tag{4.3}$$

and

$$w(t) = \sum_{n=1}^{\infty} \frac{a_n g k_n \sinh k_n(h+z)}{\sigma_n \sinh k_n h} \sin(\vec{k}_n \cdot \vec{x} - \sigma_n t + \varepsilon_n)$$

$$= \sum_{n=1}^{\infty} \frac{g k_n \sinh k_n(h+z)}{\sigma_n \sinh k_n h} \eta_n \Big|_{\varepsilon=90°} \qquad (4.4)$$

where h is the total water depth and z is the depth of interest measured positively upward from the still water level.

The terms

$$\frac{g k_n \cosh k_n(h+z)}{\sigma_n \sinh k_n h} \qquad (4.5)$$

and

$$\frac{g k_n \sinh k_n(h+z)}{\sigma_n \sinh k_n h} \quad , \qquad (4.6)$$

represent the transfer functions relating the horizontal and vertical velocities to $\eta(t)$.

## B. LIMITATIONS OF FIRST ORDER WAVE THEORY

In the formulation of linear wave theory, the boundary conditions are linearized in order to obtain an analytical solution. In the linearization, it is assumed that the amplitude, a, is small compared to the wave length, L, that is, $a/L << 1$.

Higher order solutions to the boundary value problem, generally obtained by perturbation analysis, give a better

representation of a constant profile wave. However, the nonlinearities introduced in the solution precludes their use where the principle of superposition is invoked. This in turn eliminates their generalization to a stochastic process.

Dean (1968) analyzed the various wave theories with respect to how well they fitted both the dynamic and kinematic free surface boundary conditions. He showed that first order theory provided a good solution to the wave equation for waves of permanent form having small steepness in intermediate water depths (the assumption of linear theory stated above).

The conditions prevailing during this experiment fell within these limitations. The rms wave height averaged 0.27 meters with a mean period of 16 seconds corresponding to a deepwater wavelength of 209 meters in 19 meters of water. Hence, if linear theory provides a reasonable approximation for the average wave conditions, the superposition of a large number of components, each described by linear theory, should provide an even better description.

## V. THEORETICAL CONSIDERATIONS OF DATA PROCESSING BY STATISTICAL ANALYSIS

The digitized records were spectrally analyzed using the methods of Blackman and Tukey (1958) and utilizing the IBM Model 360/67 computer at the Naval Postgraduate School.

### A. COMPUTATION OF THE ENERGY-DENSITY SPECTRUM

The covariance function $\phi_{xx}(\tau)$ of time series random data describes the general dependence of the values of the data at one time on the values at another time for the same data set. In integral form

$$\phi_{xx}(\tau) = \lim_{T\to\infty} \frac{1}{T} \int_0^T x(t)\, x(t+\tau)\, dt \qquad (5.1)$$

which is the average of the product of the value of a data point x(t) with that of an adjacent point at time $\tau$ later. The resulting average product will approach the exact auto-correlation function as T approaches infinity.

When using a covariance function generated with a finite data set, it is necessary to apply a lag window to $\phi_{xx}(\tau)$. A Parzen window, as used in this analysis, has the desirable property of no negative side lobes thus eliminating any possible numerical instability which might arise due to resonance effects of the side lobes. This is particularly critical in computing cross-spectra. The Parzen window is defined as:

$$P(\tau) = 1 - 6(\tau/T_m)^2 + 6(\tau/T_m)^3 \qquad \tau = 0,1,2,\ldots,T_m/2$$

$$= (1 - (\tau/T_m))^3 \qquad \tau = T_m/2 + 1,\ldots,T_m$$

$$= 0 \qquad \tau = T_m$$

(5.2)

where $T_m$ is the total lag time.

The energy-density spectrum as computed from the Fourier transform of the covariance function with the Parzen window applied to correct for finite record length is

$$\Phi_{xx}(f) = \int_{-\infty}^{\infty} P(\tau)\, \phi_{xx}(\tau)\, e^{-i2\pi f\tau}\, d\tau \quad , \qquad (5.3)$$

where f denotes a particular frequency.

The energy-density spectrum is the statistical estimate of the energy-density distribution in the various frequency bands comprising the spectrum and the area under an energy density spectrum is equal to twice the variance of the random variable. With respect to the wave height spectrum, the area is proportional to the total potential energy-density of the sea surface elevation, while the area under the velocity spectrum is proportional to the total kinetic energy-density.

## B. COMPUTATION OF THE CROSS-SPECTRAL DENSITY

The cross-covariance function is similar to the covariance fucntion with the exception that it compares two time records lagged by a time interval $\tau$. Thus, in integral form

$$\phi_{xy}(\tau) = \lim_{T\to\infty} \frac{1}{T} \int_0^T x(t)\, y(t+\tau)\, dt \ . \qquad (5.4)$$

If x and y are statistically independent and the mean of both x and y is zero, $\phi_{xy}(\tau) = 0$ for all f. If not, $\phi_{xy}(\tau)$ is equal to the product of the means. The lag window considerations for a finite record length are identical to those for the covariance function. The cross-spectral density is therefore the Fourier transform of the Parzen window lagged cross-covariance function

$$\Phi_{xy}(f) = \int_{-\infty}^{\infty} P(\tau)\, \phi_{xy}(\tau)\, e^{-i2\pi f\tau}\, d\tau \qquad (5.5)$$

The cross-spectrum can be defined in terms of its real and imaginary parts since, unlike the energy-density spectrum, it is not an even function. Thus

$$\Phi_{xy}(f) = C_{xy}(f) - iQ_{xy}(f) \qquad (5.6)$$

where the real part of $\Phi_{xy}(f)$ is the co-spectrum

$$C_{xy}(f) = 2 \int_0^{\infty} [\phi_{xy}(\tau) + \phi_{xy}(-\tau)] \cos(2\pi f\tau)\, d\tau \ , \qquad (5.7)$$

and the imaginary part the quadrature spectrum

$$Q_{xy}(f) = 2 \int_0^{\infty} [\phi_{xy}(\tau) - \phi_{xy}(-\tau)] \sin(2\pi f\tau)\, d\tau \ . \qquad (5.8)$$

C. COMPUTATION OF COHERENCY

A useful quantity arising out of the computation of the cross- and energy-density spectra is the coherency. Coherency is defined as

$$\gamma^2_{xy}(f) = \frac{[\Phi_{xy}(f)]^2}{\Phi_{xx}(f)\ \Phi_{yy}(f)} \quad , \tag{5.9}$$

where

$$0 \leq \gamma^2_{xy}(f) \leq 1 \ . \tag{5.10}$$

When $\gamma^2_{xy}(f) = 1$, for all f, the two records x and y are fully coherent and statistical dependence can be assumed. On the other hand, if $\gamma^2_{xy}(f) = 0$ for all f, x and y are statistically independent. Bendat and Piersol (1966) attribute coherency values less than unity to three possible causes: the system is not linear, extraneous noise is present in the measurements, or the output response is due to more than one input function.

D. COMPUTATION OF PHASE ANGLE

The cross-spectral phase angle represents the average angular difference by which the cross-correlated components of y(t) lead those of x(t) in each spectral frequency band. The phase angle can be computed using the co- and quadrature-spectra

$$\varepsilon_{xy}(f) = \arctan\ [Q_{xy}(f) \ / \ C_{xy}(f)] \ . \tag{5.11}$$

## E. PROBABILITY DENSITY FUNCTION OF THE SEA SURFACE AND INDUCED WATER PARTICLE FLUCTUATIONS

The probability density function, p(x), of random data describes the probability that the data will assume a value within some defined range at any instant of time. Mathematically

$$p(x) = \lim_{dx \to 0} \frac{\text{Prob}[x<x(t)<(x+dx)]}{dx} = \lim_{dx \to 0} \frac{1}{dx} \left[\lim_{T \to \infty} \frac{T_x}{T}\right] \qquad (5.12)$$

where $T_x$ is the amount of time that x(t) falls in the range (x, x+dx) during an observation time T.

For this experiment, the sea surface displacement was assumed to be the sum of an infinite number of independent components of random phase. Under these conditions the measured frequency distribution of the sea surface displacement tends to be Gaussian. For zero mean the Gaussian probability density function is given by

$$p_G(\xi) = \frac{1}{2\pi} e^{\xi^2/2} \qquad (5.13)$$

where $\xi$ is equal to the value of the measured quantity divided by the standard deviation. However, if the non-linearities of the boundary condition become important, departures from Gaussian are expected. Longuet-Higgins (1963) showed for "moderately" non-linear swell in deep water that the probability distribution of $\eta$ is better described by the Gram-Charlier probability density function. $p_{GC}(\xi)$ is given by:

$$p_{GC}(\xi) = p_G(\xi)\left[1.0 + \frac{m_3}{24} H_3 + \left(\frac{m_4}{24} H_4 + \frac{m_3^2}{72} H_6\right) + \ldots\right]. \quad (5.14)$$

Here the $m_i$'s are cumulants with $m_3$ being the skewness of the data record, $m_4$ the kurtosis minus three, and $H_n$ the Hermite polynomials of degree n. The Hermite polynomials are generated from

$$H_n = \xi^n - \frac{n(n-1)}{1!}\frac{\xi^{n-2}}{2} + \frac{n(n-1)(n-2)(n-3)}{2!}\frac{\xi^{n-4}}{2^2} - \ldots \quad . \quad (5.15)$$

Therefore

$$H_3 = \xi^3 - 3 \quad ,$$

$$H_4 = \xi^4 - 6\xi^2 + 3 \quad ,$$

and

$$H_6 = \xi^6 - 15\xi^4 + 45\xi^2 - 15 \quad . \quad (5.16)$$

If the distribution of $\xi$ is Gaussian, the skewness is zero and the kurtosis is equal to three which results in these and all higher order cumulants being zero making

$$p_{GC}(\xi) = p_G(\xi) \quad .$$

Kinsman (1960) made measurements of wind generated waves and showed their distribution was only approximately Gaussian and better approximated by the Gram-Charlier distribution. He found the distribution exhibited a positive skewness and attributed this skewness to the physical fact that waves have a distinct tendency to form short sharp crests and long shallow troughs.

F. GOODNESS-OF-FIT TEST

The chi-square goodness-of-fit test is used to compare a measured probability density function (PDF) to a theoretical one. A statistic with an approximate chi-squared distribution is calculated as a measure of the discrepancy between an observed PDF and the theoretical PDF. The chi-squared parameter is:

$$\chi^2 = \sum_{i=1}^{J} \frac{(f_i - F_i)^2}{F_i} \tag{5.17}$$

where $f_i$ is the observed frequency of occurence, $F_i$ the theoretical frequency of occurence, and J is the number of intervals into which the frequency distribution is divided. If a calculated distribution matches exactly a theoretical distribution the chi-squared parameter is zero.

Two methods can be used to calculate the chi-squared parameter for the goodness-of-fit test. In the first method, the $\xi$-axis of the PDF is divided into J intervals of equal size. The $f_i$'s in this case represent the number of data points in each interval between divisions and $f_i$ varies across the distribution. In the second method, the PDF is divided into J intervals of equal probability density, each containing approximately an equal number of data points in $f_i$. Williams (1950) showed that to give the test sufficient power the number of intervals, J, should be given by

$$J = 2 \sqrt[5]{\frac{2(n-1)^2}{c^2}} \tag{5.18}$$

where n is the number of time samples. C, under the null hypothesis, is the cutoff value for the level of significance which as used in this analysis was taken as 0.05.

## VI. ANALYSIS OF DATA

The analog data were digitized at 0.2 second intervals. The relationship between the upper limit of the bandwidth to be investigated, $f_c$, and the sampling interval $\Delta t$, is

$$\Delta f_c = \frac{1}{2\Delta t} . \qquad (6.1)$$

Here $f_c$ is the Nyquist frequency which in this experiment was established at 2.5 Hz. This was sufficiently high to avoid aliasing or folding problems. The maximum lag time was chosen as consistent at 10 percent of the record length. This results in twenty degrees of freedom for each computed spectra. The 80 percent confidence limits for twenty degrees of freedom are between 0.71 and 1.60 of the measured spectral estimates according to the chi-squared distribution. Because the record lengths were different for each run, there was a different frequency resolution for each run. The frequency resolution for each run is shown on the respective figures.

### A. VERTICAL VELOCITY MEASUREMENTS

The predicted and measured vertical velocity energy-density spectra, and the phase angle, and coherence-spectra of the wave height and vertical velocity were computed for runs two through six at the depths shown in Table I.

1. Predicted and Measured Vertical Velocity Energy-Density Spectra

The vertical velocities were predicted using (4.4). The predicted vertical velocity-spectrum was determined from:

$$|w(f)|^2 = \left[\frac{2\pi}{f} \frac{\sinh k(h+z)}{\sinh kh}\right]^2 |\eta(f)|^2 \qquad (6.2)$$

The term in brackets is the square of the transfer function, (4.6), relating the vertical velocity to $\eta$.

Measured vertical velocity energy-density spectra, for Runs Two and Six, are shown in Figures (11) and (12). The principle energy band was from 0.04 to 0.37 Hz as determined from the wave spectra. For Run Six, depth 5.70 meters, the theoretical values of the vertical velocity spectrum were within three to five percent of the measured vertical velocity spectrum values over a frequency range of 0.04 to 0.34 Hz. The true error of the velocities is the square-root of the spectral differences and was approximately two percent. This is within the combined error of the wave and velocity meters; hence most of the measured energy-density within this bandwidth was wave induced with relatively little spectral energy-density being due to turbulence.

On the other hand, for Run Number Two (the run of deepest depth at 14.62 meters) the absolute difference between the measured and theoretical spectra was small over the much narrower bandwidth of 0.05 to 0.19 Hz. The large absolute difference between the measured and theoretical

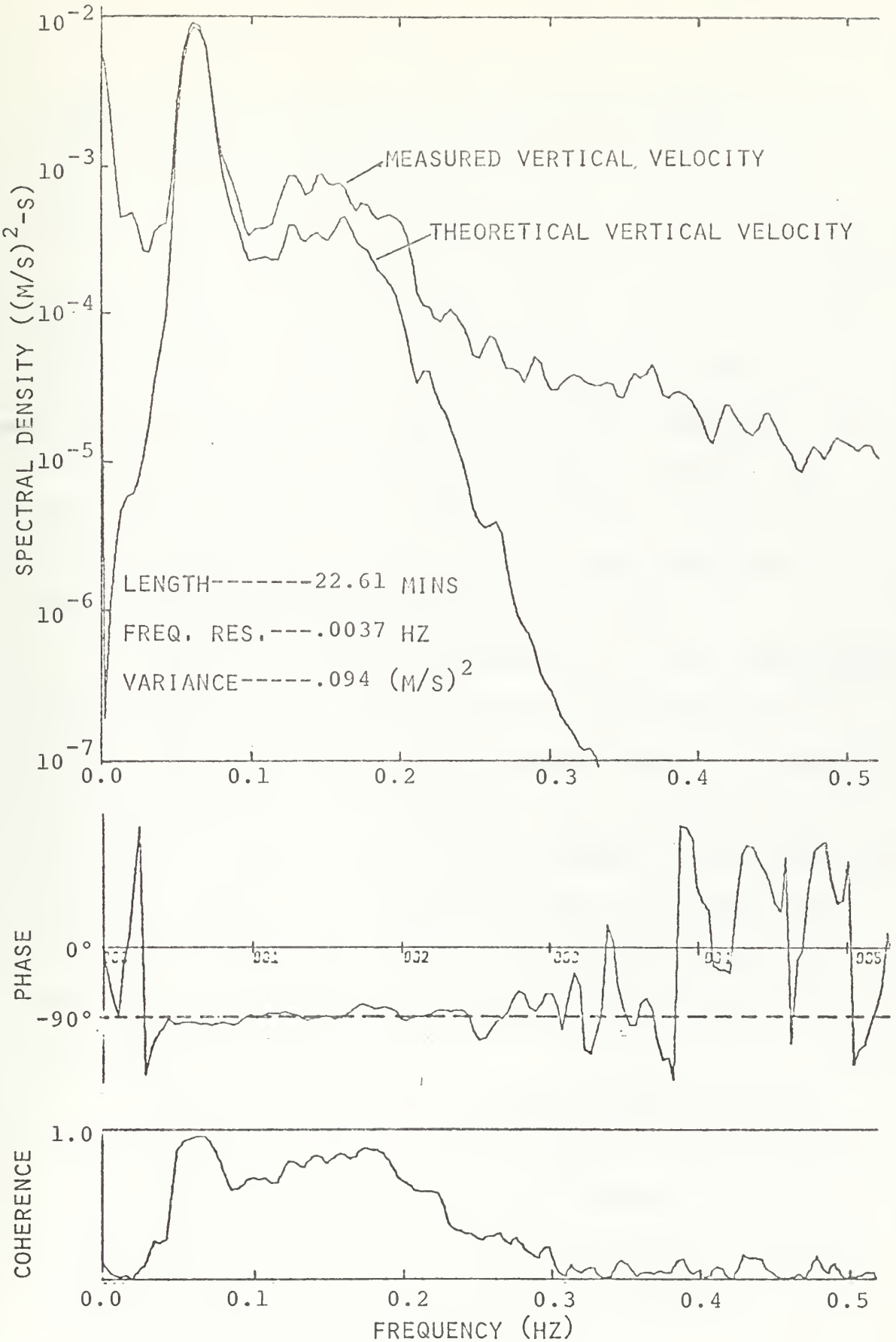


Figure 11. Measured and Theoretical Vertical Velocity Spectra for Run Number Two. Depth 14.62 Meters.

spectra at high frequencies for both runs indicates that beyond 0.19 Hz for Run Number Two and 0.34 Hz for Run Number Six, that most of the energy was due to turbulence.

The decrease of wave induced motion with increased depth can also be seen by comparing the vertical velocity spectra for the two runs. For Run Number Six there was a peak in energy due to a three second wave component. This peak was not present in the spectra for Run Number Two. That the energy present at this frequency and depth was due to turbulence can be seen by the large deviation between the measured and theoretical spectra.

Like the spectral energy-density in the wave induced part of the spectrum, the turbulent energy-density level was one order of magnitude less for Run Number Two compared to Run Number Six. This indicates that turbulent motion decreased at the same rate as wave induced motion under the particular conditions of moderate swell, low winds, and intermediate water depth and that the intensity of the turbulence is associated with the rms value of the wave-induced motion.

A measure of the total energy available in the measured spectra is given by the variance. The value of the variance, and therefore the total kinetic wave-induced energy present, decreased with increasing depth. There is almost an order of magnitude difference between the two values indicating a rapid decrease in energy with depth as predicted by theory.

2. Coherence of the Wave Height and Measured Vertical Velocity

The coherence spectra are also shown in Figures (11) and (12). In general, the coherence was 0.8 or greater throughout the range of significant wave induced energy-density. This means that there is a high correlation between the waves and wave-induced vertical motion and that relatively little of the energy in the significant energy-density band was due to turbulence, but instead, was wave-induced.

3. Phase Angle Between Wave Height and the Vertical Velocity

The phase angle theoretically leads wave height by 90 degrees. The two computed phase spectra in Figures (11) and (12) further reflect the accuracy of linear theory at both shallow and deep depths.

Bordy (1972) encountered the greatest departure from linear wave theory in the computation of the phase angle. Much effort was expended during the course of this experiment to ensure that phase angle errors due to experimental technique were minimized. The concurrance of the constant phase angle with depth further supports linear theory. It is felt that keeping the wave sensor directly over the flowmeter was the sole reason for the difference in the results obtained in this research as compared with those of Bordy.

4. Comparison of Phase Angle and Coherence for Different Depths

As can be seen from Figure (13), there is a definite relation between the phase angle for a given frequency and

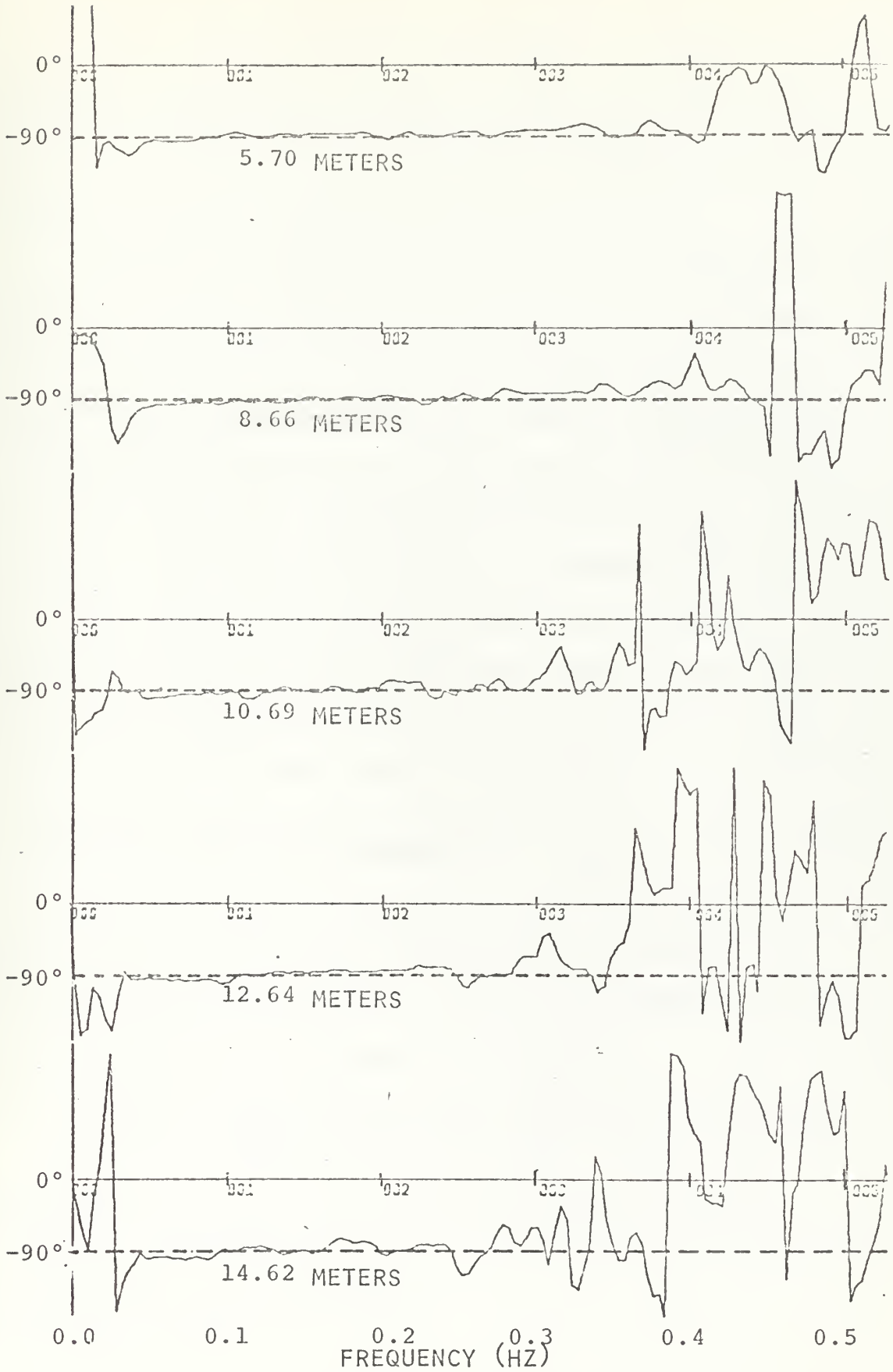


Figure 13. Vertical Phase Spectra for Runs Two Through Six.

the depth of measurement. The 90 degree phase shift was observed to a period of 0.4 Hz at the shallowest depth, but only as far as 0.25 Hz for the deepest case.

The upper frequency limit of high coherence also decreases with increasing depth as illustrated in Figure (14). Both of these phenomena can be explained by linear theory. Linear theory predicts decreasing particle motion with increasing depth due to a passing wave and that for a given depth the lower frequency waves induce greater particle motion. This is reflected in the coherence and phase plots. The highest frequency at which the coherence approached one and at which the phase compared well with theory for all analyzed runs corresponded with the onset of significant turbulent energy contribution.

## B. HORIZONTAL VELOCITY MEASUREMENTS

The predicted and measured total horizontal velocity energy-density spectra were computed for Run Number One. The phase angle and coherence spectra were computed using the wave height and v-component of velocity.

### 1. Predicted and Measured Horizontal Velocity Spectra

The total theoretical horizontal velocity was computed from (4.3). The theoretical energy-density spectrum of the total wave-induced horizontal velocity was calculated from the expression

$$|\vec{u}(f)|^2 = \left[\frac{f}{2\pi} \frac{\cosh k(h+z)}{\sinh kh}\right]^2 |n(f)|^2 . \qquad (6.3)$$

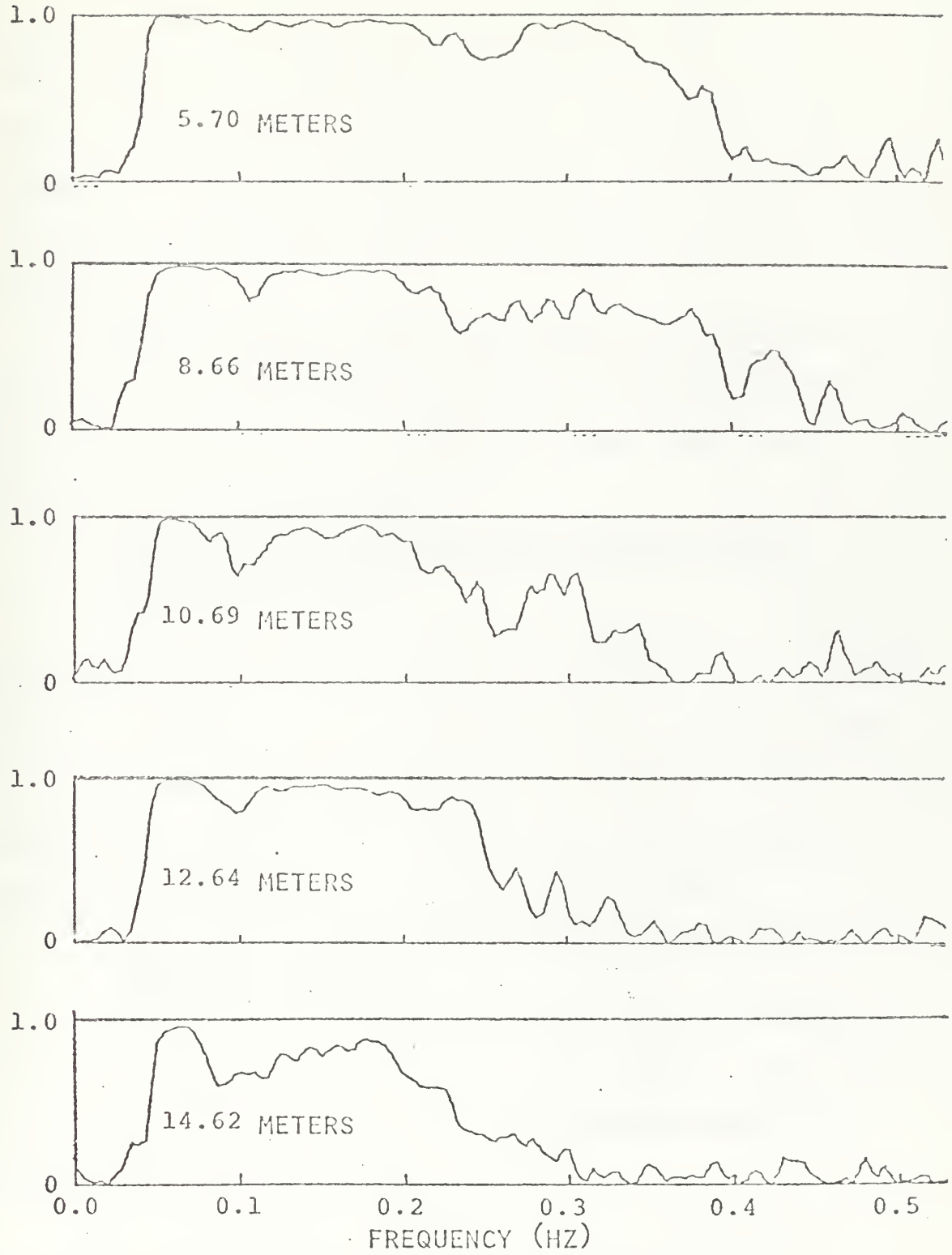


Figure 14. Vertical Coherence Spectra for Runs Two Through Six.

The term in brackets is (4.5), the transfer function relating the total horizontal velocity to η. The total spectrum was found by calculating the individual u- and v-component spectra and summing over the frequency band of interest. The spectra are illustrated in semi-log format in Figure (15).

The difference between the spectra at the peak was found to be about 12 percent, giving an absolute value of the difference of about 3.5 percent in the significant energy-density frequency band.

2. Coherence of Wave Heights and Measured Total Horizontal Velocity

The coherence (of η and the v-component of velocity) was calculated to be greater than 0.9, Figure (15), throughout the significant energy frequency band of 0.03 to 0.07 Hz. This high coherence was due to the fact that the v-component of velocity was primarily wave-induced and the turbulent contribution to the spectrum was small.

3. Phase Angle Between Wave Height and the Total Horizontal Velocity

The theoretical phase angle for the wave height and the v-component of velocity is zero degrees. This was found to be true in this case as illustrated again in Figure (15).

## C. PROBABILITY DENSITY FUNCTIONS AND STATISTICS OF THE DATA SETS.

A probability density function was computed for each measured quantity for the six runs. The points comprising

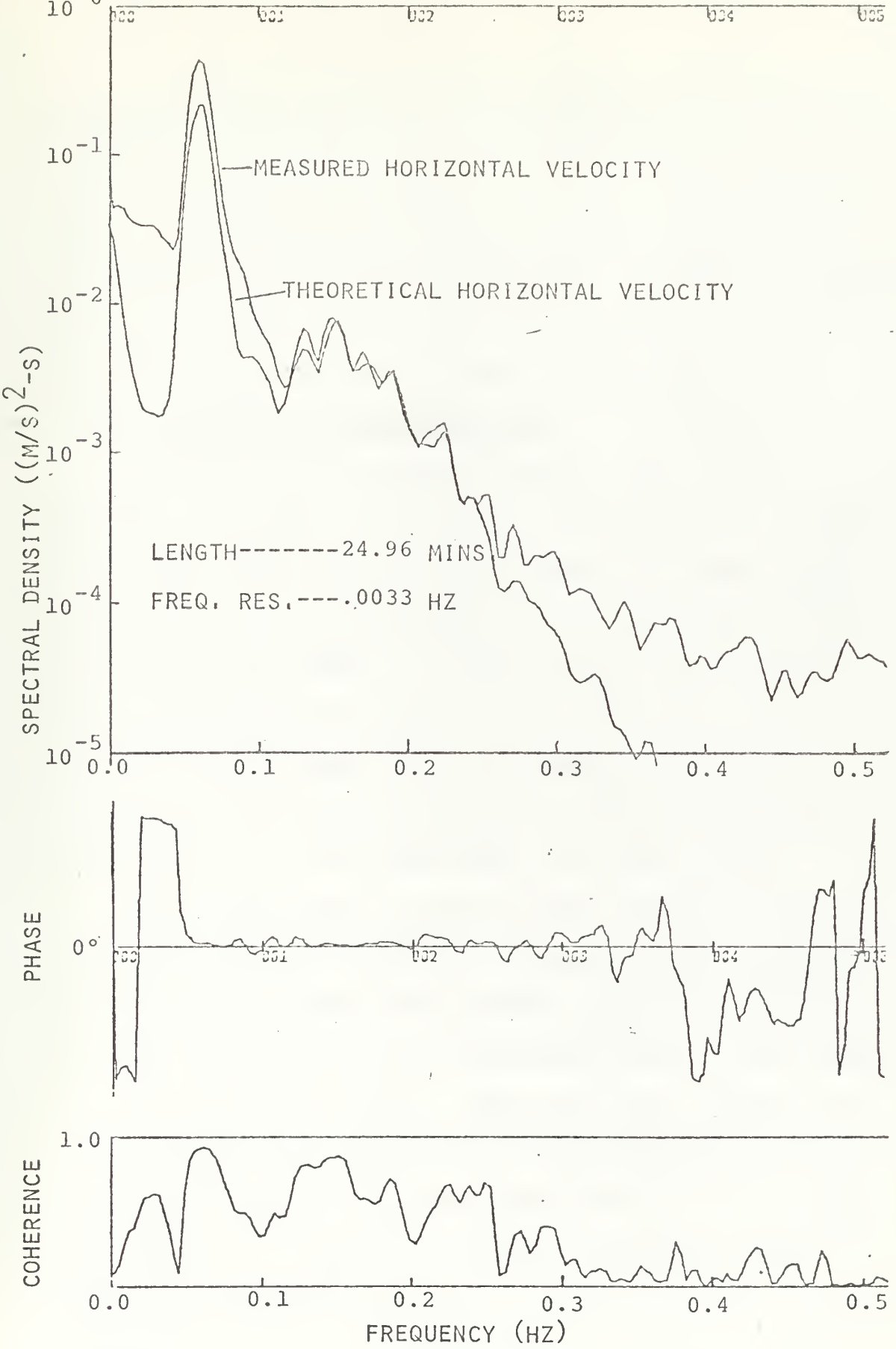


Figure 15. Measured and Theoretical Horizontal Velocity Spectra for Run Number One. Depth 7.04 Meters.

a histogram of the data sets were plotted against both a Gaussian and a Gram-Charlier distribution. The chi-squared goodness-of-fit test was computed for both theoretical distributions. The statistics, variance, standard deviation, skewness, and kurtosis were also computed for all eighteen data sets. These results are listed in Table IV.

1. Probability Density Functions

A typical PDF is shown in Figure (16). It is known that the ocean's surface has approximately a Gaussian distribution. However, the non-linearities of the surface introduce values of the skewness and kurtosis that deviate from Gaussian and result in a Gram-Charlier distribution. This is explained by the physical fact that waves tend to form short, sharp crests and long troughs. For the waves this produces a positive skewness, indicating more values in the time series below mean water level than above.

It follows that the wave induced particle motion should follow the same behavior. However, of the eighteen data sets analyzed, three did not have positive skewness. These three were the velocity components u and w from Record Five and w from Record Three. Why this is so, despite the fact that all the wave records were positively skewed, remains unexplained. A possible explanation could be that this peculiarity is caused by internal waves which were prevalent during the experiment.

TABLE IV

| RUN/ DEPTH (m) | QUANTITY | VARIANCE | STANDARD DEVISTION | SKEWNESS | KURTOSIS | CHI-SQUARED PARAMETER GAUSSIAN | CHI-SQUARED PARAMETER GRAM-CHAR |
|---|---|---|---|---|---|---|---|
| 1/ | u-comp. | .536 | .732 | .023 | 2.65 | 113.21 | 57.27 |
| 7.04 | v-comp. | 1.39 | 1.18 | .117 | 2.73 | 137.14 | 91.36 |
| | wave | .393 | 2.21 | .154 | 2.95 | 80.12 | 49.53 |
| 2/ | u-comp. | .414 | .644 | .109 | 2.68 | 155.64 | 126.11 |
| 14.62 | w-comp. | .094 | .307 | .214 | 3.10 | 124.21 | 50.38 |
| | wave | .451 | 2.35 | .078 | 2.65 | 144.58 | 93.53 |
| 3/ | u-comp. | .396 | .630 | .020 | 2.85 | 50.40 | 47.98 |
| 12.64 | w-comp. | .167 | .409 | -.042 | 3.08 | 74.31 | 68.84 |
| | wave | .418 | 2.24 | .074 | 2.97 | 45.57 | 38.65 |
| 4/ | u-comp. | .451 | .672 | .012 | 3.10 | 59.52 | 52.65 |
| 10.69 | w-comp. | .255 | .505 | .024 | 2.88 | 59.31 | 55.43 |
| | wave | .454 | 2.38 | .115 | 2.86 | 59.34 | 38.65 |
| 5/ | u-comp. | .353 | .594 | -.084 | 2.85 | 89.46 | 77.58 |
| 8.66 | w-comp. | .423 | .650 | -.024 | 2.83 | 33.85 | 29.94 |
| | wave | .327 | 2.00 | .124 | 2.85 | 67.63 | 45.06 |
| 6/ | u-comp. | .532 | .730 | .142 | 2.88 | 61.17 | 42.15 |
| 5.70 | w-comp. | .699 | .836 | .013 | 2.84 | 52.73 | 48.88 |
| | wave | .668 | 2.62 | .038 | 3.02 | 48.98 | 46.88 |

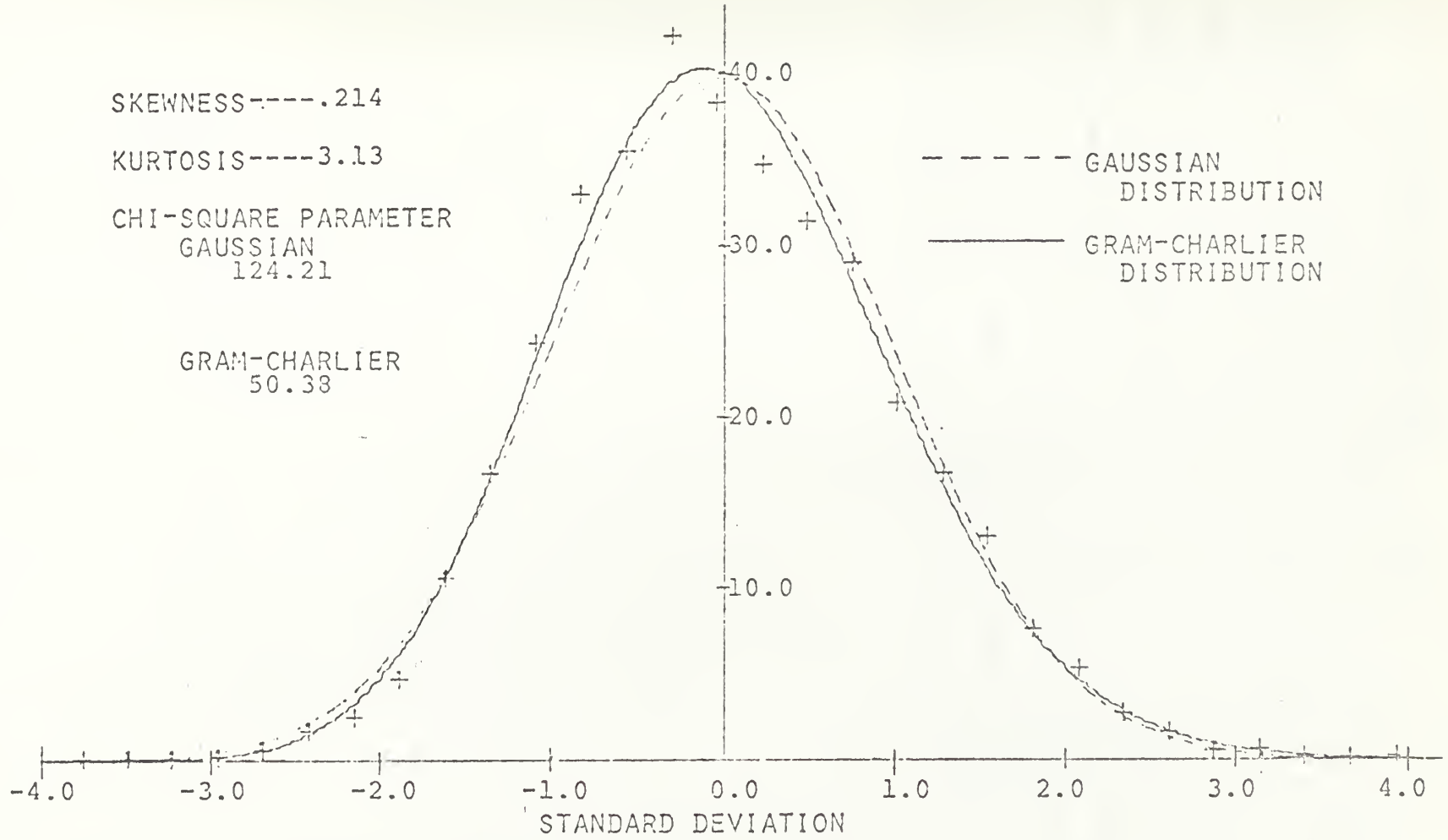


Figure 6. Gaussian and Gram-Charlier Distribution Plotted Against Data PDF for the w-Component of Velocity Run Two. Depth 14.62 Meters, 8 June 1972.

2. Goodness-of-Fit Test

The chi-squared goodness-of-fit test was used to compare the computed PDF to both the Gaussian and Gram-Charlier distributions for all eighteen data sets. Qualitatively, based on the smaller chi-squared values obtained from a comparison of the PDF with the Gram-Charlier distribution, it can be stated that all eighteen records more closely fit the Gram-Charlier distribution than the Gaussian. The chi-squared parameter for all eighteen data sets is also listed in Table IV.

## VII. CONCLUSIONS

The measurements in this research were made under conditions of moderate swell and low wind velocity. Wave height was measured with a penetrating wave staff and water particle motion measured with an electromagnetic flowmeter.

### A. ENERGY-DENSITY SPECTRA

The wave-induced vertical velocity energy-density spectra were computed for six depths. The frequency of the peak energy-density remained constant with depth. However, the significant energy-density of the wave-induced motion at high frequency decreased with increasing depth according to the attenuation aspects of linear theory. The magnitude of the energy-density spectra also decreased with increasing depth according to theory. It was noted that the lowest frequency at which turbulence contributed significantly to the spectra shifted to lower frequencies with increased depth. The intensity of the turbulent contribution decreased with depth and appears associated with the variance of the wave-induced velocities.

### B. COHERENCE

Coherence of the wave height and wave-induced velocities was computed to be greater than 0.85 throughout the range of significant energy-density. The upper frequency limit of high coherence decreased with increasing depth. The value of the upper limit was established at the frequency where

turbulence became an important factor in the energy-density. The near unity values of coherence over the band of significant spectral-density imply a near linear process between wave height and induced water particle motion. It is felt that the small irregularities in coherence in the significant energy-density band were due to turbulence.

C. PHASE ANGLE

The computed phase angle spectra of the wave height and induced water particle motions were consistent with the theory at all depths for both vertical and total horizontal velocity cases. This is the part of the analysis where Bordy (1972) encountered the greatest deviation from theory. It is imperative that the wave staff be directly over the flowmeter in order that there be no phase error. A similar decreasing upper frequency limit with increasing depth for consistent phase angle values was present as it was for both the coherence and the energy-density spectra.

D. STATISTICAL INTERFERENCES

The probability density functions of all measured quantities were qualitatively found to be better described by the Gram-Charlier distribution than by the Gaussian using the chi-squared goodness-of-fit test. The variance of the vertical velocities, a measure of the kinetic energy present, decreased with increasing depth which is consistent with linear theory. The skewness of the wave height frequency distribution was found to be positive in all cases as a

consequence of the fact that waves tend to have short, sharp crests and elongated troughs. The values of skewness, with few exceptions, were found to be positive for the wave-induced quantities as well. These exceptions might be explained by the presence of internal waves.

## LIST OF REFERENCES


1. Abramowitz, M. and Stegun, I.A., Handbook of Mathematical Functions, U.S. Governement Printing Office, 1964.

2. Bendat, K.R. and Piersol, A.G., Measurement and Analysis of Random Data, pp. 234-237, Wiley, 1966.

3. Blackman, R.B. and Tukey, J.W., The Measurement of Power Spectral, Dover Publication, Inc. New York, New York, 1959.

4. Bordy, W.B., Spectral Measurements of Water Particle Velocities Under Waves, M.S. Thesis, Naval Postgraduate School, Monterey, California, 1972.

5. Bowden, K.F. and Fairbairn, L.A., Measurements of Turbulent Fluctuation and Reynolds Stress in a Tidal Current, Royal Society of London Proceedings, Ser. A237, pp. 422-438, 1956.

6. Bowden, K.F. and White, R.A., "Measurements of the Orbital Velocities of Sea Waves and Their Use in Determining the Directional Spectrum", Geophysical Journal of the Royal Astronautical Society, Vol. 12, pp. 33-54, 1966.

7. Cox, D.R. and Lewis, P.A.W., The Statistical Analysis of Series of Events, pp. 134-152, Wiley, 1966.

8. Hastings, C., Approximations for Digital Computers, pp. 150-154, Princeton University Press, 1955.

9. Inman, D.L. and Nasu, N., "Orbital Velocity Associated with Wave Action Near the Breaker Zone", U.S. Army Corp of Engineers, Beach Erosion Board, Technical Memorandum Nol 79, March 1956.

10. Kinsman, G., Wind Waves, p. 134 and pp. 342-346, Prentice Hall, 1965.

11. Longuet-Higgins, M.S., "The Effect of Non-Linearities on Statistic Distributions in the Theory of Sea Waves", Journal of Fluid Mechanics, V. 17, Part 3, pp. 459-480, November 1963.

12. Miller, R.L. and Zeigler, J.M., "The Internal Velocity Field in Breaking Waves", 9th Conference on Coastal Engineering National Council for Wave Research, Lisbon, Portugal, 1964.

13. Nagata, Y., Observation of Wave Motion by Electromagnetic Current Meter, Proceedings Meetings on Coastal Engineering, Japan Society of Civil Engineering, 1963.

14. Nagata, Y., "The Statistical Properties of Orbital Wave Motion and Their Application for the Measurement of Directional Wave Spectra", Journal of the Oceanographical Society of Japan, Vo. 19, pp. 169-181, (1964a, 1964b)

15. Phillips, O.M., The Dynamics of the Upper Ocean, pp. 154-158, Cambridge University Press, 1966.

16. Seitz, R.C., "Measurements of a Three-Dimensional Field of Water Velocities at a Depth of One Meter in an Estuary", Journal of Marine Research, Vo. 29, pp. 140-150, 1971.

17. Shonting, D.H., "Measurements of Particle Motions in Ocean Waves," Journal of Marine Research, Vol. 25, pp. 162-181, 1971.

18. Simpson, J.H., "Observation of the Directional Characteristics of Waves", Geophysical Journal of the Royal Astrounautical Society, Vol. 17, pp. 93-120, 1969.

19. Williams, C.A., Jr., "On the Choice of the Number and Width of Classes for Chi-Square Test of Goodness-of-Fit", Journal of the American Statistical Association, Vol. 45, pp. 77-86, March 1950.

## INITIAL DISTRIBUTION LIST

| | | No. Copies |
|---|---|---|
| 1. | Defense Documentation Center<br>Cameron Station<br>Alexandria, Virginia 22314 | 2 |
| 2. | Library, Code 0212<br>Naval Postgraduate School<br>Monterey, California 93940 | 2 |
| 3. | Oceanographer of the Navy<br>The Madison Building<br>732 N. Washington Street<br>Alexandria, Virginia 22217 | 1 |
| 4. | Department of Oceanography, Code 58<br>Naval Postgraduate School<br>Monterey, California 93940 | 3 |
| 5. | Commander, Navy Ship Systems Command<br>Code 901<br>Department of the Navy<br>Washington, D.C. 20305 | 1 |
| 6. | Dr. Ned A. Ostenso<br>Deputy Director (acting)<br>Code 480 D<br>Ocean Science and Technology Division<br>Office of Naval Research<br>Arlington, Virginia 22217 | 1 |
| 7. | Dr. Albert D. Kirwan, Jr.<br>Program Director/Physical Oceanography<br>Ocean Science and Technology Division<br>Office of Naval Research<br>Arlington, Virginia 22217 | 1 |
| 8. | LCDR Jon W. Carlmark (USN)<br>Project Office<br>Code 485<br>Ocean Science and Technology Division<br>Office of Naval Research<br>Arlington, Virginia 22217 | 1 |
| 9. | Professor H. Medwin, Code 61Md<br>Department of Physics<br>Naval Postgraduate School<br>Monterey, California 93940 | 1 |

10. Asst. Professor Noel E. Boston, Code 58Bb — 1
Department of Oceanography
Naval Postgraduate School
Monterey, California 93940

11. Asst. Professor Edward B. Thornton, Code 58Tr — 5
Department of Oceanography
Naval Postgraduate School
Monterey, California 93940

12. Lieutenant Richard F. Krapohl (USN) — 1
USS Connole (DE 1056)
FPO New York, New York 09501

13. Mr. David Halpern — 1
Pacific Oceanographic Laboratories
University of Washington
Seattle, Washington 98105

14. Professor Vytautas Klemas — 1
College of Marine Studies
University of Delaware
Newark, Delaware 19711

15. Dr. Robert G. Dean — 1
Department of Civil and Ocean Engineering
University of Florida
Gainesville, Florida 32601

16. Mr. J.A. Battjes — 1
Department of Civil Engineering
Delft University of Tech.
25 Oostplantsoen
Delft, The Netherlands

17. Prof. J. Van De Kreeke — 1
Department of Ocean Engineering
School of Marine and Atmospheric Sciences
University of Miami
10 Rickenbacker Causeway
Miami, Florida 33149

18. Mr. Thorndike Saville, Director — 1
Coastal Engineering Research Center
Department of The Army
5201 Little Falls Road N.W.
Washington, D.C. 20016

| | | |
|---|---|---|
| 19. | Dr. D. Lee Harris<br>Coastal Engineering Research Center<br>Department of The Army<br>5201 Little Falls Road, N.W.<br>Washington, D.C. 20016 | 1 |
| 20. | Chief of Naval Research<br>Geography Programs, Code 414<br>Office of Naval Research<br>Washington, D.C. 22217 | 1 |
| 21. | Dr. Earnst Breeding<br>Naval Mine Defense Laboratory<br>Panama City, Florida | 1 |
| 22. | Prof. Warren C. Thompson, Code 58Th<br>Department of Oceanography<br>Naval Postgraduate School<br>Monterey, California 93940 | 1 |
| 23. | Lieutenant Michael W. Bordy (USN)<br>USS Implicit (MSO 455)<br>FPO San Francisco, California 96601 | 1 |

Security Classification

DOCUMENT CONTROL DATA - R & D

(Security classification of title, body of abstract and indexing annotation must be entered when the overall report is classified)

ORIGINATING ACTIVITY (Corporate author)

Naval Postgraduate School
Monterey, California 93940

2a. REPORT SECURITY CLASSIFICATION

Unclassified

2b. GROUP

REPORT TITLE

Wave-Induced Water Particle Motion Measurements

DESCRIPTIVE NOTES (Type of report and inclusive dates)

Master's Thesis; December 1972

AUTHOR(S) (First name, middle initial, last name)

Richard Francis Krapohl

| REPORT DATE | 7a. TOTAL NO. OF PAGES | 7b. NO. OF REFS |
|---|---|---|
| December 1972 | 66 | 19 |

| CONTRACT OR GRANT NO. | 9a. ORIGINATOR'S REPORT NUMBER(S) |
|---|---|
| PROJECT NO. | |
| | 9b. OTHER REPORT NO(S) (Any other numbers that may be assigned this report) |

DISTRIBUTION STATEMENT

Approved for public release; distribution unlimited.

| SUPPLEMENTARY NOTES | 12. SPONSORING MILITARY ACTIVITY |
|---|---|
| | Naval Postgraduate School<br>Monterey, California 93940 |

ABSTRACT

Simultaneous measurements of wave height and two orthogonal water particle velocities were made at six elevations in nineteen meters of water using a penetrating wave staff and an electromagnetic flowmeter. Moderate swell and low wind conditions prevailed during the experiment. The measured wave-induced velocities were two to four percent greater than those predicted using linear wave theory. Coherence of the wave height and wave-induced velocities in the significant energy-density range was computed to be over 0.85, indicating that the motion was almost totally wave induced. At higher frequencies it was apparent that the motion was primarily turbulence. Phase spectra computed for the measured wave heights and orbital velocities compared very well with linear theory. Measured frequency distributions were compared to both Gaussian and Gram-Charlier distributions using the chi-squared goodness-of-fit test. Qualitatively, the Gram-Charlier distribution gave the better fit to the data.

DD FORM 1 NOV 68 1473 (PAGE 1)

S/N 0101-807-6811



Security Classification

A-31408

| KEY WORDS | LINK A | | LINK B | | LINK C | |
|---|---|---|---|---|---|---|
| | ROLE | WT | ROLE | WT | ROLE | WT |
| Water Particle Motion | | | | | | |
| Spectral Measurements | | | | | | |
| Linear Wave Theory | | | | | | |
| Power Spectra | | | | | | |
| Random Description of Sea Surface | | | | | | |

141293
Thesis
K852 Krapohl
c.1 Wave-induced water particle motion measurements.